Modeling the formation and fate of the near-surface temperature maximum in the Canadian Basin of the Arctic Ocean

Michael Steele,[1] Wendy Ermold,[1] and Jinlun Zhang[1]

Received 12 November 2010; revised 6 August 2011; accepted 8 September 2011; published 12 November 2011.

[1] A numerical model is used to investigate the time and space extent of the near-surface temperature maximum (NSTM) of the Canadian Basin of the Arctic Ocean over the years 2000–2009. The NSTM is formed from local summertime absorption of solar radiation which, in some circumstances, descends through the fall and early winter to form a warm subsurface layer just below the winter mixed layer. We find that winter survival of this layer is confined largely to the Beaufort Gyre of the Canadian Basin, where Ekman convergence and downwelling push the summer warm layer down below the winter mixing depth. In recent years, summer stratification has increased, downwelling has accelerated, and the NSTM has warmed as the sea ice cover in the Beaufort Gyre has thinned. The result is a strengthening NSTM which contained enough heat by the end of winter 2007/2008 to melt about 20 cm of sea ice. Northwest of Alaska the model also simulates a second, deeper temperature maximum layer that forms from advection of saltier summer Pacific water. However, this layer is difficult to adequately resolve and maintain given the model's resolution.

Citation: Steele, M., W. Ermold, and J. Zhang (2011), Modeling the formation and fate of the near-surface temperature maximum in the Canadian Basin of the Arctic Ocean, *J. Geophys. Res.*, *116*, C11015, doi:10.1029/2010JC006803.

1. Introduction

[2] Summer sea ice retreat in the Arctic Ocean has accelerated in recent years [e.g., *Serreze et al.*, 2007], a response to long-term warming trends as well as shorter-term atmospheric forcing [*Lindsay and Zhang*, 2005; *Min et al.*, 2008; *Nghiem et al.*, 2007]. This allowed 500% more solar energy into the surface layers of the Beaufort Sea in the summer of 2007 (relative to the 1979–2005 mean), resulting in anomalous ocean warming and sea ice melting [*Perovich et al.*, 2007, 2008; *Steele et al.*, 2008, 2010]. Figure 1 shows the situation at the end of summer 2007, using both model output (described in section 2) and observed data.

[3] *Jackson et al.* [2010] discussed how summertime warming of the upper layers of the Arctic Ocean has intensified in recent years, and how this warming is affecting subsurface layers through the following winter season. Their study focused on the Canada Basin (a subregion of the Canadian Basin), using summertime hydrographic temperature and salinity data as well as similar year-round data obtained from ice-tethered drifting buoys. They defined a shallow near-surface temperature maximum (NSTM) that forms within an initially cold, near-freezing mixed layer in contact with sea ice, via the subsurface absorption of solar radiation. The NSTM deepens within the Beaufort Gyre and, in recent years, can survive through the winter. This is in contrast to an earlier study by *Maykut and McPhee* [1995] who identified a Canadian Basin NSTM in the 1970s that disappeared by the end of October.

[4] Figure 2 shows the evolution of temperature and salinity profiles at four locations (see Figure 1) using a model described in section 2. The upper ocean warms well above freezing in areas where sea ice melts away completely by September (points 1 and 2). In the fall, ice growth creates convective overturning which erodes the upper portion of the warm layer, leaving an NSTM that deepens over time (point 1) within the envelope of the September temperature profile (i.e., at no depth in the upper 100 m is there a temperature increase above the September value). A signature of warm Atlantic water is evident at point 1 as increasing temperatures below 50 m depth; other points in Figure 2 also have this layer, but at depths deeper than 100 m. Summer heating is particularly strong at point 2, but so is convective mixing such that the NSTM has eroded completely by January 2008. Fall temperature profiles at this location deepen below the September envelope, a result of lateral advection as discussed below.

[5] The other two points shown in Figure 2 lie under the multiyear ice pack, where the surface temperature is constrained to freezing even in summer. At point 3, the NSTM cools and deepens through the fall, but does not disappear completely by January 2008. The survival of this heat through the winter is a main focus of this study. Point 4 lies at a comparable latitude to point 3, but it is farther into the ice pack interior (Figure 1) and thus the NSTM is cooler.

[6] In this study, we use a numerical model to better define the space and time boundaries of the NSTM. For example, it is not clear from previous work whether the

[1]Applied Physics Laboratory, Polar Science Center, University of Washington, Seattle, Washington, USA.

0148-0227/11/2010JC006803

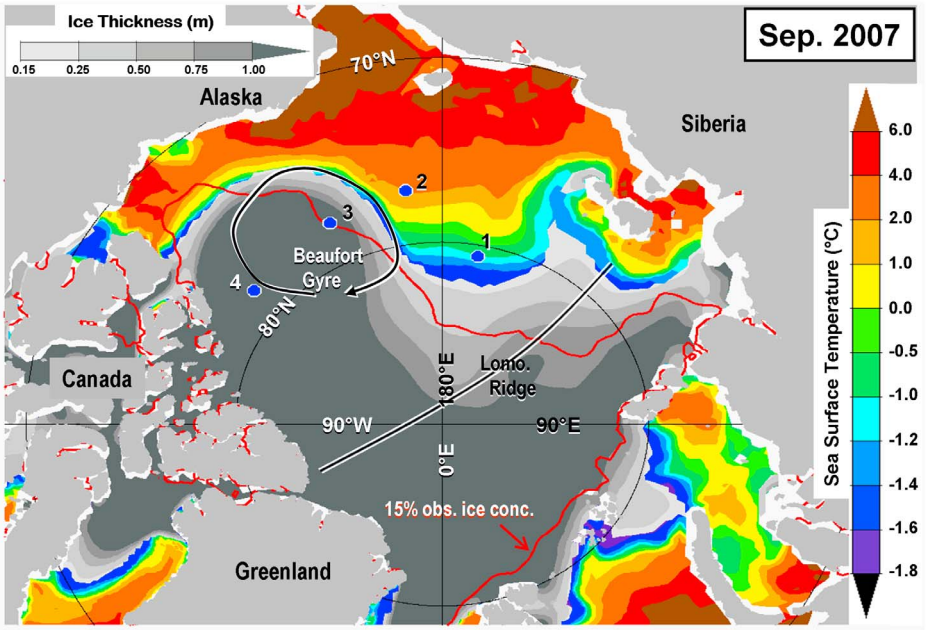

Figure 1. September 2007 mean modeled sea surface temperature (color contours) and modeled sea ice thickness (gray contours). The model is described in section 2. Also shown (red line) is the September 2007 mean 15% sea ice concentration contour from passive microwave satellite data (National Snow and Ice Data Center; see ftp://sidads.colorado.edu/pub/DATASETS/seaice/polar-stereo/nasateam/final-gsfc/readme.txt) and four model grid points (blue dots) used in Figures XX. The approximate mean annual location of the anticyclonic circulation of sea ice and upper ocean currents known as the Beaufort Gyre is marked, although its spatial extent and amplitude undergo considerable interannual variability [*Yang*, 2009]. The Canadian Basin lies on the Canadian/Alaskan/eastern Siberian side of the Lomonosov (Lomo) Ridge.

NSTM extends into other parts of the Arctic Ocean beyond the Canada Basin. We also examine the dynamics of its formation and persistence. Why is there an NSTM in some places, but not in others? Some implications of this new temperature maximum for the sea ice mass balance and for water mass definitions in the upper Arctic Ocean are also discussed. Section 2 outlines the model used in this analysis. Section 3 then explores the space and time extent of the NSTM for a case study, the fall and winter of 2007/2008, and includes a validation comparing model output and observed hydrographic data. We discuss the dynamics of NSTM formation in section 4, and then in section 5 we show a longer-term perspective on NSTM extent and properties. In section 6 we focus on the relationship between the NSTM and summer Pacific water. We close with a discussion of our results in section 7.

2. Model

[7] We use output from a coupled sea ice – ocean model of the Arctic seas, the Pan-Arctic Ice–Ocean Modeling and Assimilation System (PIOMAS) of *Zhang and Rothrock* [2003]. The ocean component is based on the Parallel Ocean Program (POP) ocean model [e.g., *Smith et al.*, 1992], which is coupled to a multicategory thickness and enthalpy distribution (TED) sea ice model [*Hibler*, 1980; *Zhang and Rothrock*, 2001]. The POP model is a B-grid Bryan–Cox–Semtner–type ocean model [*Bryan*, 1969; *Semtner*, 1976] with an implicit free-surface formulation of the barotropic mode and model adaptation to parallel comput-

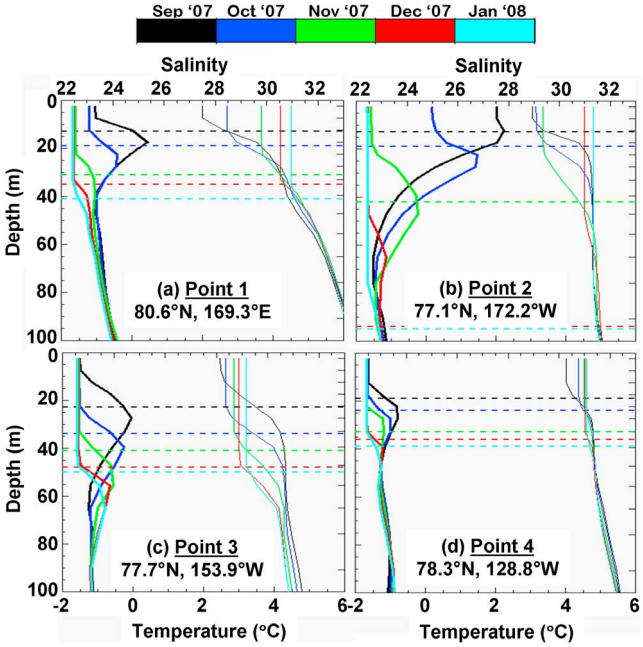

Figure 2. Monthly mean temperature profiles (heavy solid lines) and salinity profiles (lighter solid lines) from four model grid points in the Canadian Basin (see Figure 1) in the fall and early winter of 2007/2008. The model is described in section 2. Also shown is the maximum daily mean mixed layer depth in each month (dashed lines) and model depth levels on the right-hand vertical scale.

ing. The TED sea ice model has 12 categories each for ice thickness, ice enthalpy, and snow depth [*Zhang et al.*, 2000]. Mean horizontal resolution of both ice and ocean models is about 22 km, with higher resolution near Greenland where the North Pole is displaced by a linear orthogonal transformation. Resolution across Bering Strait is three grid cells for scalars (temperature and salinity) and two for velocity, which provides realistic volume transport [*Zhang et al.*, 2008] although higher resolution would probably enhance the accuracy of near-coastal flows and eddies. The ocean model's vertical dimension has 30 levels of increasing thickness with depth, starting with six 5 m thick levels in the upper 30 m, then increasing gradually to 10 m thick by 65 m depth, 18.5 m thick at 91 m depth, and eventually 700 m thick at 4200 m depth. Ocean vertical mixing follows the K profile parameterization (KPP), while ocean horizontal Laplacian mixing coefficients depend on the grid cell area, with diffusivity of 4–6 × 10^5 cm^2 s^{-1} in the Canadian Basin and viscosity 100 times higher. Ice-ocean heat flux parameterizations were discussed in the work of *Hibler* [1980] and *Hibler and Bryan* [1987]. Open boundary conditions for sea surface height and ocean velocity, temperature, and salinity are specified along the model's southern boundary at 43°N from a global version of the model [*Zhang*, 2005]. Daily mean NCEP/NCAR reanalysis data are used as atmospheric forcing; that is, 10 m surface winds, 2 m surface air temperature (SAT), specific humidity, precipitation, evaporation, downwelling longwave radiation, sea level pressure, and cloud fraction. Cloud fraction and SAT are used to calculate downwelling shortwave radiation following *Parkinson and Washington* [1979]. No shortwave radiation is allowed to penetrate through snow on sea ice, but some is allowed to penetrate through sea ice and below the ocean surface, with a vertical attenuation coefficient in ice of 1.5 m^{-1} [*Maykut and Untersteiner*, 1971]. For the ocean, monthly climatological fields (averaged over 1988–2009) of attenuation that vary with phytoplankton concentration are taken from output from a similar biophysical model [*Zhang et al.*, 2010b]. Canadian Basin values range from 0.04 m^{-1} in winter to 0.14 m^{-1} in spring and summer. Snow albedo is set at 0.80 (0.75 if melting), sea ice albedo is 0.70 (0.65 if melting), and ocean albedo is 0.10 [*Maykut*, 1982]. Climatological river discharge (i.e., no interannual variability) is provided as in the work of *Hibler and Bryan* [1987]. The freezing point of seawater is computed as −0.0575 times the salinity. The model has the capability to assimilate ice concentration and ocean sea surface temperature observations through a nudging algorithm, but this function is not implemented in this study. The model has been validated using sea ice concentration, sea ice thickness, sea ice motion, ocean hydrography, and ocean transports [*Lindsay et al.*, 2009; *Zhang et al.*, 2008; *Zhang and Steele*, 2007]. In particular, vertical ocean mixing has been optimized to the observed hydrography in the Arctic Ocean, with specific attention to the Canadian Basin [*Zhang and Steele*, 2007]. In this study we use the KPP vertical mixing scheme, with a "background" vertical diffusivity coefficient of 0.02 cm^2 s^{-1}. Further model validation of NSTM properties is provided in section 3.

[8] The model was initially forced with repeated 1948 NCEP/NCAR fields [*Makshtas et al.*, 2007] for 30 years to equilibrate toward conditions during this year, and then forced with atmospheric fields from 1948 to 2009. Initial sea ice was at rest, with thickness of 2.6 m where the 1 January 1948 surface air temperature was equal to or colder than −20°C. Initial ocean temperature and salinity were taken from the 1982 version of the World Ocean Atlas [*Levitus*, 1982], with no initial ocean motion. For this study, model output was saved as daily averages over the years 2000–2009.

[9] Mixed Layer Depth (MLD) is used in this study in several ways. There are many methods to define MLD. Here we choose the most common "increment" method, using density instead of the common temperature criterion because of the influence of salinity on density at cold Arctic temperatures. We define MLD as the shallowest depth at which the potential density exceeds 0.2 kg m^{-3} of the mean potential density over the upper 10 m, using model temperature and salinity profiles linearly interpolated to 1 m resolution. Averaging over the upper 10 m is a common strategy to deal with the frequently noisy near-surface ocean density profile, although it may lead to an overestimate of the summer MLD in the Canadian Basin [*Toole et al.*, 2010]. A density increment of 0.2 kg m^{-3} is appropriate when analyzing model profiles that represent averages over space and time [*de Boyer Montegut et al.*, 2004]. Reducing our increment by even a factor of ten reduces the estimated MLD by only a few meters in the Canadian Basin, given the highly stratified conditions even in winter [*Toole et al.*, 2010].

3. Mapping the NSTM 2007–2008

[10] The NSTM of the Canadian Basin is the temperature maximum (T_{max}) that forms in the Arctic Ocean from the local absorption of solar shortwave radiation into a cold mixed layer. Thus, it was defined by *Jackson et al.* [2010] as the shallowest T_{max} that satisfies three criteria. These are:

[11] Criterion 1. The T_{max}'s temperature above freezing must be greater than 0.2°C.

[12] Criterion 2. The T_{max}'s temperature above freezing must be more than 0.1°C warmer than an immediate underlying temperature minimum.

[13] Criterion 3. The T_{max}'s salinity must be less than 31.

[14] Criterion 1 filters out weak signals. Criterion 2 ensures the presence of a true temperature minimum below the T_{max}. Criterion 3 is designed to filter out the temperature maximum found in summer Pacific water, which is often defined by salinities greater than 31 [*Shimada et al.*, 2001; *Steele et al.*, 2004]. For this study, our first step was to identify all temperature maxima in the upper 200 m on the model's vertical grid, where a local maximum was defined as a temperature greater than those at model grid points immediately above and below by 0.001°C. This is referred to as "criterion 0." Then each successive criterion was applied, until all were combined to provide a final "all criteria" NSTM.

[15] An example is provided in Figure 3. In September 2007, the modeled criteria 0 + 1 (Figure 3b) and criteria 0 + 2 (Figure 3c) NSTMs extend over the entire Arctic Ocean, with amplitudes up to and above 6°C. Under the ice pack, subsurface solar radiation penetrates into leads and through thin ice, warming a layer that resides under the cold, freezing surface. In the open water, maximum ocean temperature can be found right at the surface in early summer where ice melt-back is early. However, by September the surface starts to cool (Figures 2a and 2b) and thus an NSTM forms. Criterion 3

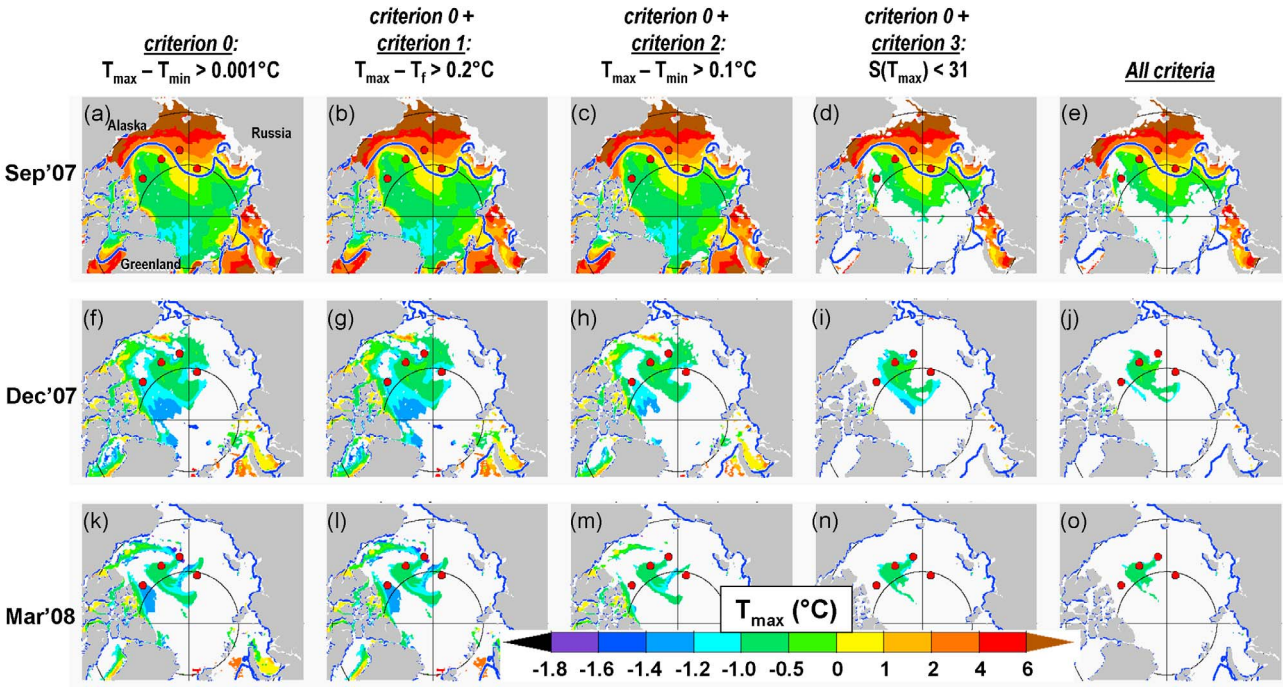

Figure 3. Definition of the NSTM, for 3 months: (a–e) September 2007, (f–j) December 2007, and (k–o) March 2008. The criteria are explained in section 3. Also shown are the modeled ice edge (blue contour) and the four locations from Figure 1 (red dots).

filters out most of the generally saltier surface waters on the Atlantic side of the basin (Figure 3d). By December 2007, the criterion 0 NSTM has cooled considerably, and its domain has shrunk. Criteria 1, 2, and 3 further reduce its extent to the central and northern Canadian Basin. In particular, criterion 3 is designed to filter out summer Pacific water, defined by the difference between Figure 3i and Figures 3f–3h. This difference is most pronounced along the Canadian Archipelago and in a roughly zonal line extending into the Canadian Basin from the north Alaskan shelf. These are the two main pathways of summer Pacific water intrusion as envisioned by *Jones et al.* [1998] and *Steele et al.* [2004] and will be discussed in further detail below. The NSTM survives through at least March 2008, although reduced in temperature and extent.

[16] For now, we will use the "all criteria" NSTM, and explore its time and space extent and evolution over the fall and winter of 2007/2008. Figure 4 shows key properties of the NSTM for September and December of 2007. Ocean currents at the depth of the NSTM are anticyclonic, a reflection of the Beaufort Gyre. The depth of the NSTM is generally quite shallow and uniform over the entire domain in early and midsummer (10–15 m depth, not shown), but by September, it has deepened in the center of the Beaufort Gyre, and this deepening continues through December. Similarly, the depth of the NSTM below the MLD is fairly uniform in the summer, but in the fall it increases in the gyre. The dynamics of this process will be discussed below.

[17] How well does the model reproduce the observed NSTM properties? This is explored in Figure 5 by comparison with data collected by ice-tethered profiler buoys [*Krishfield et al.*, 2008]. For this comparison, we applied our "all criteria" NSTM algorithm to daily mean ITP data. If an NSTM was identified, then a comparison was made if (1) the nearest model grid point for that day also had an NSTM, and (2) the modeled ice thickness was greater than 1.5 m. The latter condition ensures that the comparison is for profiles that are under ice for both ITP and model. Thus the comparison involves no interpolation; the maximum distance between a model and ITP profile is ~22 km.

[18] Figure 5 shows that the model has a T_{max} temperature bias and standard error of several tenths of a degree Celsius. It is generally too warm in summer. By December the bias is much reduced but still of the same order of magnitude as the NSTM itself. The simulated depth of the T_{max} is well represented, with a standard error of the same order as the model resolution at these depths (i.e., 5–10 m). The modeled salinity of the T_{max} is too high by 1–2, where the bias is slightly larger in the southern Beaufort Gyre, relative to the northern gyre (not shown). While the model does produce a general freshening trend (see Figure 11) such as observed in recent years [*McPhee et al.*, 2009] the pace of this freshening is underestimated by the simulation. This may be similar to the difficulty that many models have in reproducing the rapid pace of recent sea ice retreat [*Stroeve et al.*, 2007]. Our analysis below indicates that the simulation is capturing many aspects of the observed NSTM as discussed by *Jackson et al.* [2010]; however the error shown in Figure 5 indicates that further model refinement is desirable.

[19] Figure 6 shows the temporal evolution of the NSTM from summer 2007 through the end of 2008 at two locations in Figure 1. At point 2 (Figure 6a) sea ice retreats early in the summer of 2007 and as a result the ocean surface warms above 2°C [*Steele et al.*, 2008, 2010]. Maximum upper ocean heat content is reached in late September and early October. However, ice growth is strong in the fall, creating a

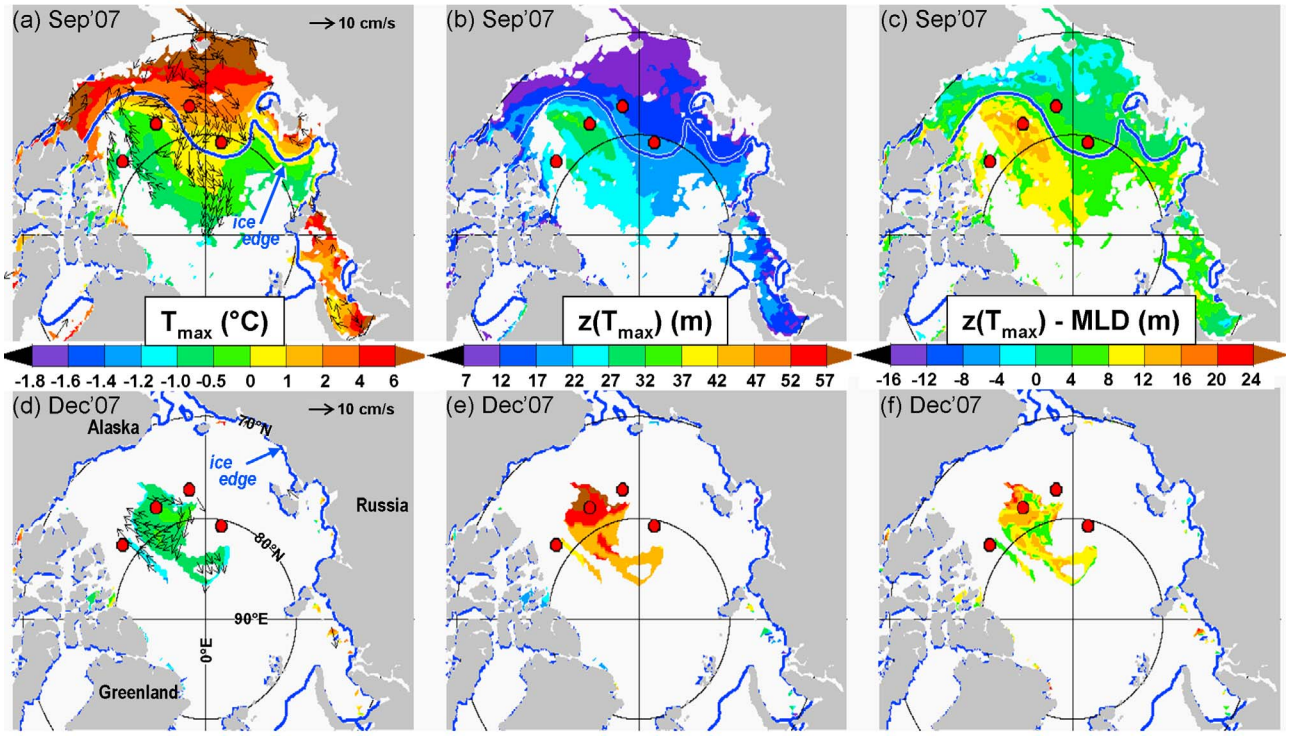

Figure 4. NSTM (a and d) temperature T_{max}, (b and e) depth $z(T_{max})$, and (c and f) depth below the mixed layer depth $z(T_{max}) - MLD$ for September 2007 (Figures 4a–4c) and December 2007 (Figures 4d–4f). Also shown are the modeled ice edge (blue contour), the four locations from Figures 1 and 2 (red dots) and, in Figures 4a and 4d, ocean velocity vectors at the NSTM depth. The NSTM here is defined using all criteria in Figure 3.

deep saline mixed layer that extracts all of the summer heat by the end of the year.

[20] At point 3 (Figure 6b), only a moderate T_{max} forms in summer 2007 under the perennial sea ice pack. Total upper ocean heat content is smaller here, relative to that at point 2, and it peaks earlier in the summer. Fall ice growth is also moderate, so that convection is weaker at this time relative to that at point 2 and the mixed layer does not deepen as far. The NSTM survives through the entire winter of 2007/2008. A further consideration of the mechanisms involved with its winter survival is presented in section 4. In summer of 2008, a new NSTM forms above the existing one, in response to ice melt and restratification of the upper ocean.

[21] By the time that ice starts growing at point 3 in September 2007, the NSTM heat content is ~270 MJ m^{-2}, which represents about 1 m of potential ice melt. Through the fall, the NSTM deepens and loses heat through the ocean surface. Some of this heat escapes directly to the atmosphere through leads, while the rest is used to reduce sea ice growth. By the end of winter in April 2008, NSTM heat content is reduced to ~60 MJ m^{-2}, which represents 20 cm of ice melt. One way to interpret this is that 20 cm of sea ice could melt if all of the heat in this warm layer were to escape to the surface (which Figure XX indicates does not happen, at least not at that time). Another interpretation is that an additional 20 cm of sea ice grew over the winter that might not have, if this heat were not sequestered below the ocean surface. Of course, some of this heat could also have escaped in the fall directly to the atmosphere through leads. Eventually, this sequestered heat mixes up into the surface layer and is lost, if not in the Beaufort Gyre then downstream in other areas of the Arctic Ocean such as the Lincoln Sea [*Steele et al.*, 2004]. It is clear that winter persistence of the NSTM has a small but interesting effect on the sea ice mass balance, a topic that we deem beyond the scope of the present work.

4. Explaining the NSTM

[22] How does the NSTM form? *Jackson et al.* [2010] ascribed its origins to the summertime absorption of solar radiation into a cold surface mixed layer in contact with sea ice. Figures 2 and 3 show that an NSTM can also form in late summer in open water areas as the stratified upper ocean cools from the surface. Either way, the formation of an NSTM relies crucially on the subsurface absorption of solar radiation, which allows subsurface heating of the cold surface mixed layer. Figure 7 confirms this, showing the result of a sensitivity experiment in which all solar radiation is absorbed at the uppermost model grid point at 2.5 m depth. In this case, more ocean heat is used to melt ice in the summer, relative to the standard case (Figure 6), and this heat is confined much closer to the surface, only reaching deeper layers via advection and diffusion. The result is that fall convection and mixing forced by ice growth and winds rather quickly cools the ocean surface down to freezing, and no wintertime NSTM forms.

[23] What causes the deepening of a temperature maximum layer? We assume an "initial condition" in late summer (here,

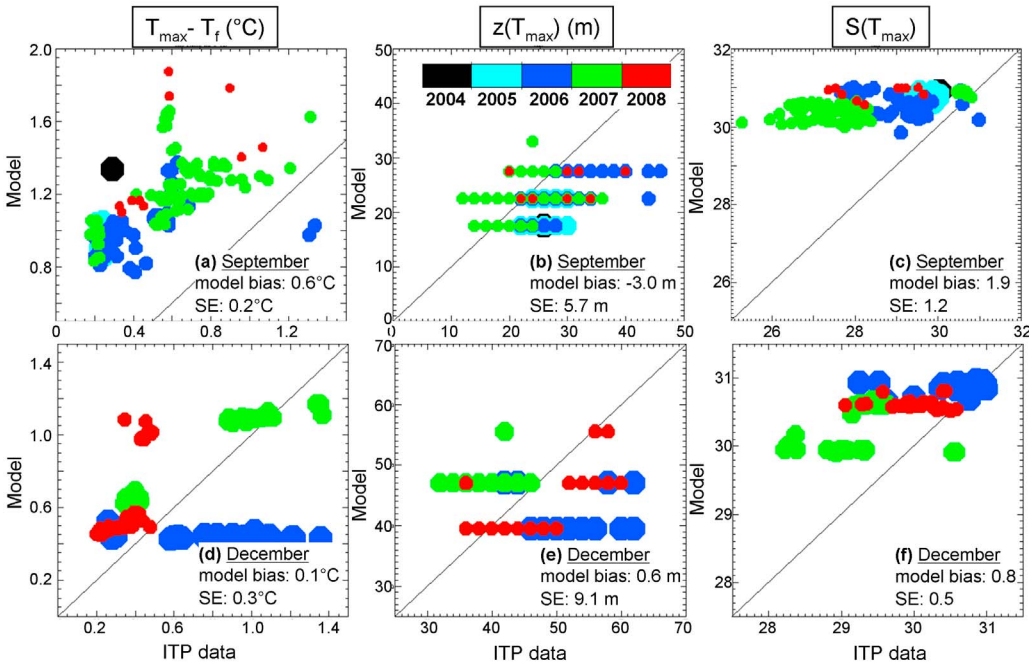

Figure 5. Comparison of model output versus data collected by ice-tethered profilers (ITPs) [*Krishfield et al.*, 2008] for three parameters: (a and d) elevation above freezing $T_{max} - T_f$, (b and e) depth of temperature maximum $z(T_{max})$, and (c and f) salinity of temperature maximum $S(T_{max})$ for September (Figures 5a–5c) and December (Figures 5d–5f) over the years 2004–2008 (color bar). Earlier data (larger dots) are overplotted by later data (smaller dots). In 2004, there is only one ITP observation (in September, black dot). Note the different scales. Also shown is the line with 1:1 slope (thin black line), the mean model bias relative to ITP values, and the standard error (SE). ITP unit numbers 1–19, 21, 23–29, 33, 34, 36, and 37 were used in this analysis. The NSTM here is defined using all criteria in Figure 3.

September 2007) in which the NSTM is warm (Figure 4a) from atmospheric heating and/or ocean advection from the south [*Steele et al.*, 2010]. There are three ways that a temperature maximum can deepen during the fall. The first is simple surface mixing of the stratified upper ocean, forced by negative buoyancy (cooling and/or salt rejection from ice growth) and/or stress (i.e., wind and/or ice motion). This erodes the top portion of the NSTM, cooling it off while lower layers remain warm. An example is provided at point 1 (Figure 2a), where the upper ocean cools from the surface, but the temperature profiles stay within the envelope of the September profile. This mechanism will generally completely erode the summer NSTM layer by the end of fall, given that typical late fall daily maximum MLDs are ≥40 m, which is the bottom of the summer NSTM layer.

[24] A second way that the surface T_{max} layer can deepen is by downwelling within the pycnocline, forced by Ekman convergence within the surface mixed layer. If this downwelling outpaces the deepening mixing layer during fall, then the T_{max} may survive through the winter. An example is provided at point 3, which lies in the center of the convergent Beaufort Gyre, as confirmed by Figure 8a. The downwelling velocity at this point is about 8 m per month in September, which explains the T_{max} deepening shown in Figure 2c.

[25] A third mechanism for T_{max} deepening is the lateral advection of dense warm water. In this case, the local surface NSTM may erode via surface mixing, but a secondary "injection" of warm subsurface water from nearby provides additional heat. An example is provided at point 2, which lies in the pathway of summer Pacific water; that is, warm ocean currents extending northwestward from Alaska [*Steele et al.*, 2010, Figure 7]. Figure 8b indicates that ocean warming from lateral heat flux convergence is generally greatest just south of the western Arctic Ocean ice edge, in keeping with previous studies of convergence in this area [*Yang*, 2009]. The area with the largest positive amplitude north and northwest of Alaska is explored in further detail in section 6. Under the ice pack, lateral heat flux convergence is quite small, indicating that T_{max} layers in this model simulation are not strongly advecting there.

5. Historical Context of the NSTM

[26] How has the NSTM changed over the first decade of the 21st century? Here we examine interannual variations in NSTM properties over this time period. Our primary focus is on the winter season, since we are concerned with the fate of ocean heat accumulated during the previous summer.

[27] Figure 9 shows how the "all criteria" NSTM December mean extent has increased, starting from essentially nothing in the year 2000 (not shown) through 2003. A small area of December NSTM appears first in 2004, and increases in extent through 2007, after which it stays relatively unchanged. The December NSTM extent since 2007 is confined to the downwelling Beaufort Gyre (Figure 8a), which suggests that

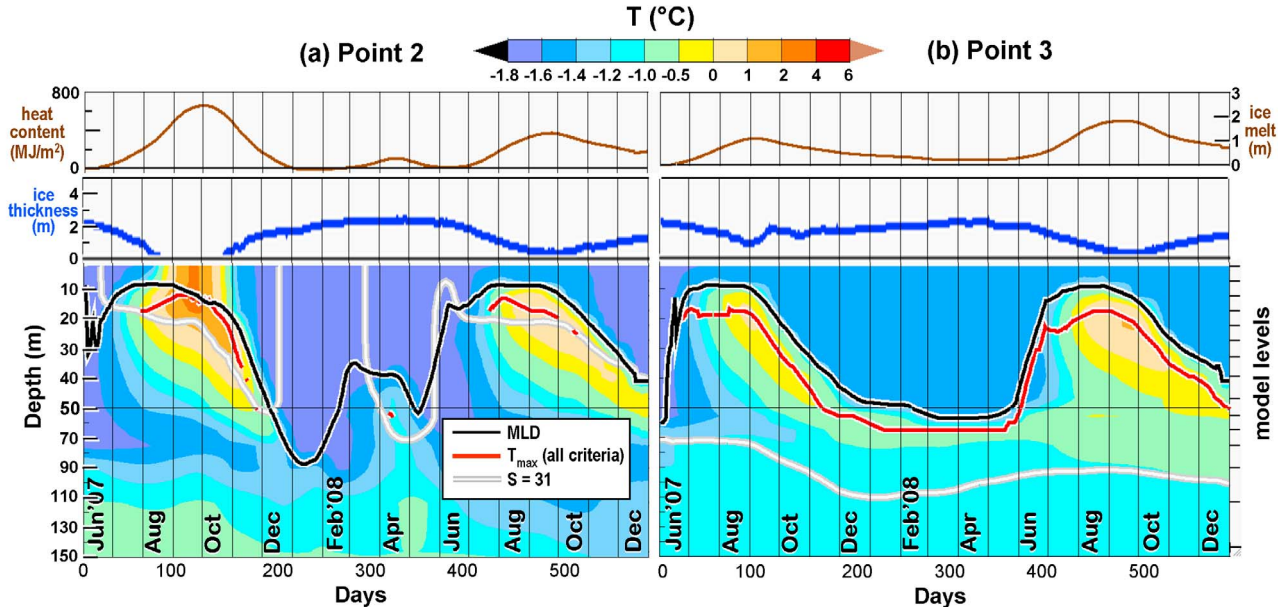

Figure 6. Modeled temperature over the upper 150 m from June 2007 through December 2008 at points 2 and 3 (see Figure 1). Note the break in the vertical depth scale at 50 m. The uppermost T_{max} (using all criteria) is shown (red solid line), as is the MLD (black line), the S = 31 contour (light gray line), the mean ice thickness (blue time series at the top), and the vertically integrated heat content down to 80 m depth relative to the value on 1 June 2007 (brown time series at the top) with an alternate scale of ice melting on the right-hand side (i.e., heat content divided by sea ice density = 900 kg m^{-3} and sea ice latent heat of fusion = 3×10^5 J kg^{-1}). Daily mean model output is used but then smoothed with a running 30 day mean boxcar filter. Model depth levels are indicated on the right-hand scale.

the "all criteria" NSTM survives through the winter only via mechanism 2 discussed in section 4; that is, by downwelling that outpaces a deepening surface mixing layer.

[28] Figure 10 shows the December NSTM extent and salinity, using criteria 1 and 2. In this plot, criterion 3 is not used, and thus temperature maxima are allowed even if they are saltier than 31. The result is a larger areal coverage, with the difference from that shown in Figure 9 representing temperature maxima with salinities great than 31. In all years, a relatively salty area extends northwestward from Alaska, where Figure 8b shows a strong advective warming signal. As discussed in detail in section 6, this area is where

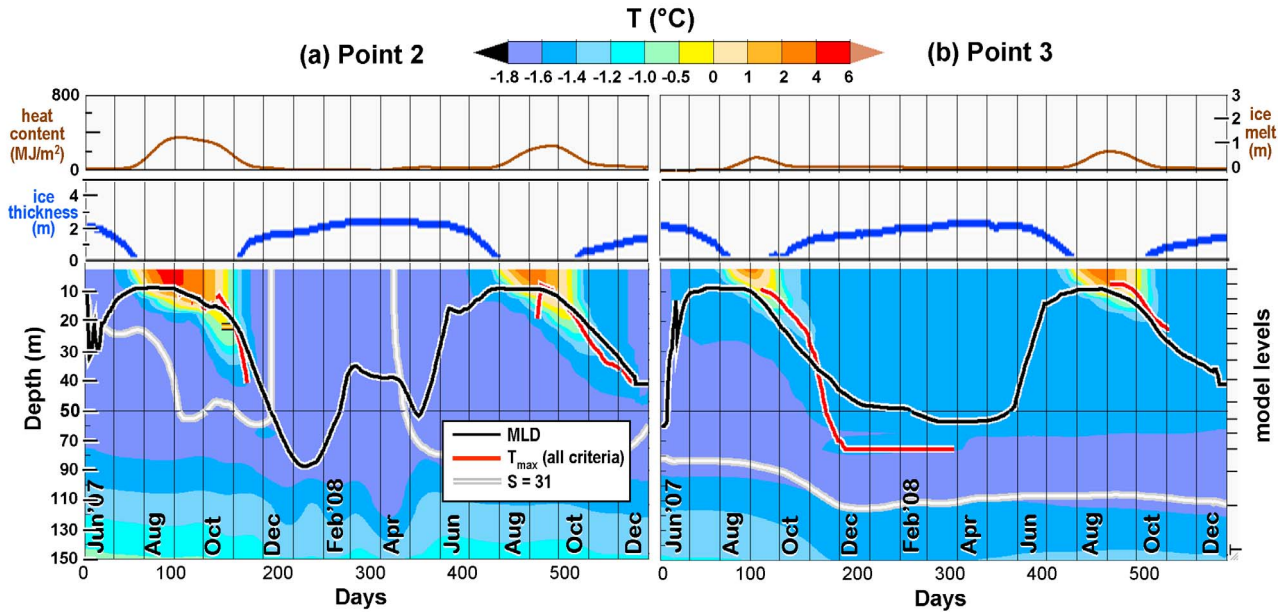

Figure 7. As in Figure 6 but with no subsurface absorption of solar radiation.

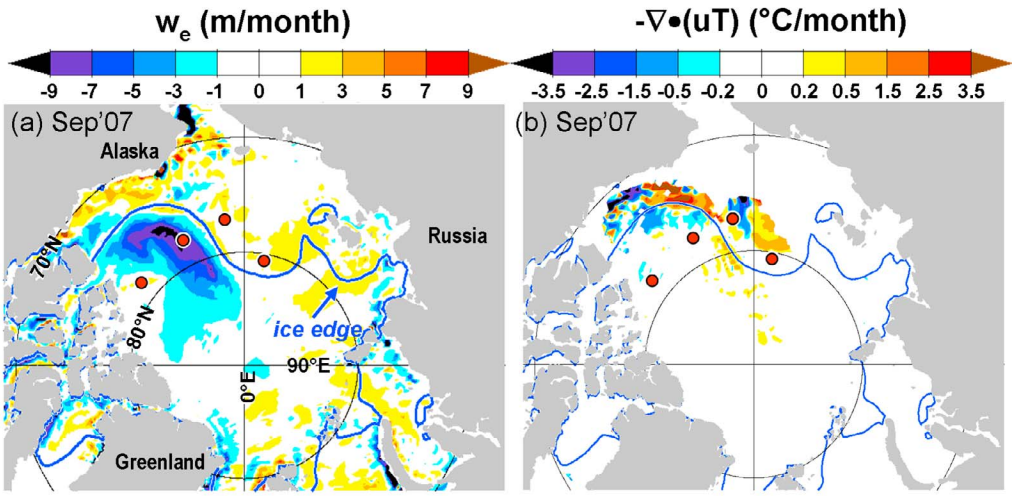

Figure 8. September 2007 modeled conditions in the upper ocean with the modeled ice edge (blue curve) and the four positions from Figures 1 and 2 (red dots). (a) Upwelling velocity at the base of the mixed layer calculated by integrating the convergence over this layer. Negative values indicate downward motion. (b) Heat flux convergence at the depth of the T_{max} (see Figure 4b), where positive values indicate ocean warming, all NSTM criteria from Figure 3 are used, and values are plotted only for locations where the total depth of the ocean is greater than 500 m.

the summer Pacific water T_{max} is forming in the model. Figure XX also shows areas with a secondary deep T_{max} (black contours) below the primary one which denote areas with either multiyear deep NSTMs or summer Pacific water, as discussed in further detail below.

[29] Figure 11 shows the evolution of the upper 150 m ocean temperature over the entire 10 years 2000–2009 at point 3 in the Beaufort Gyre. Also shown are the ice thickness and the monthly mean upwelling velocity at this location. A general trend toward thinner summer ice is evident, as is a

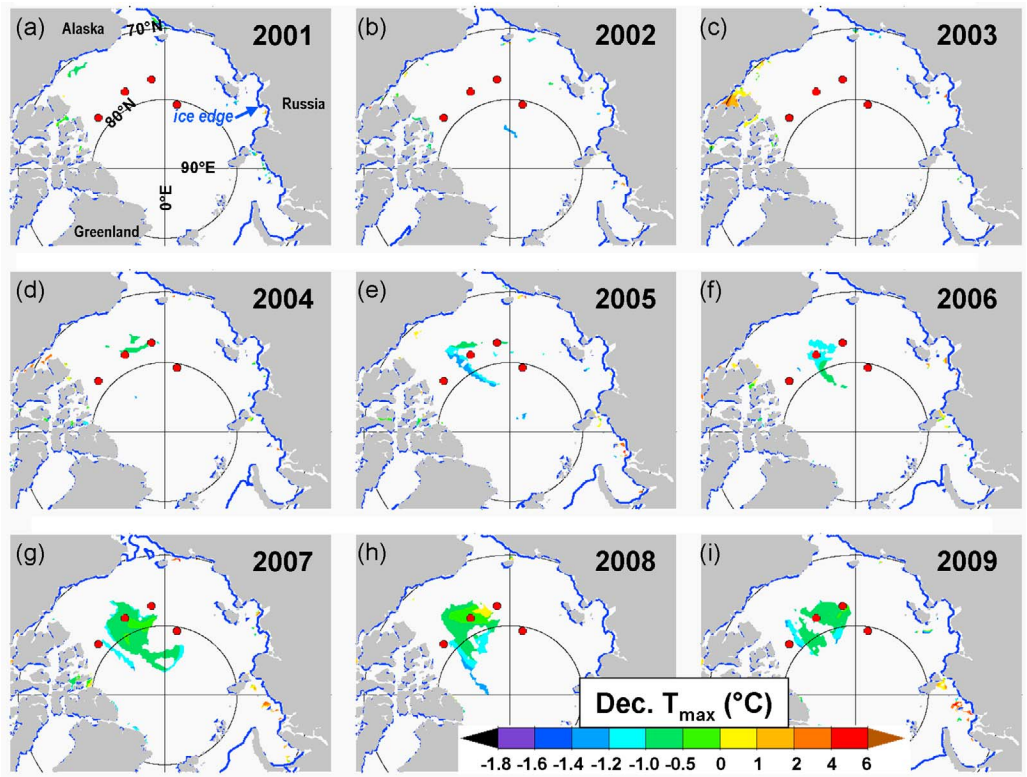

Figure 9. Temperature of the modeled December mean NSTM over the years 2001–2009 using all criteria discussed in section 3. Also shown is the modeled ice edge (blue curve) and the four positions from Figures 1 and 2 (red dots).

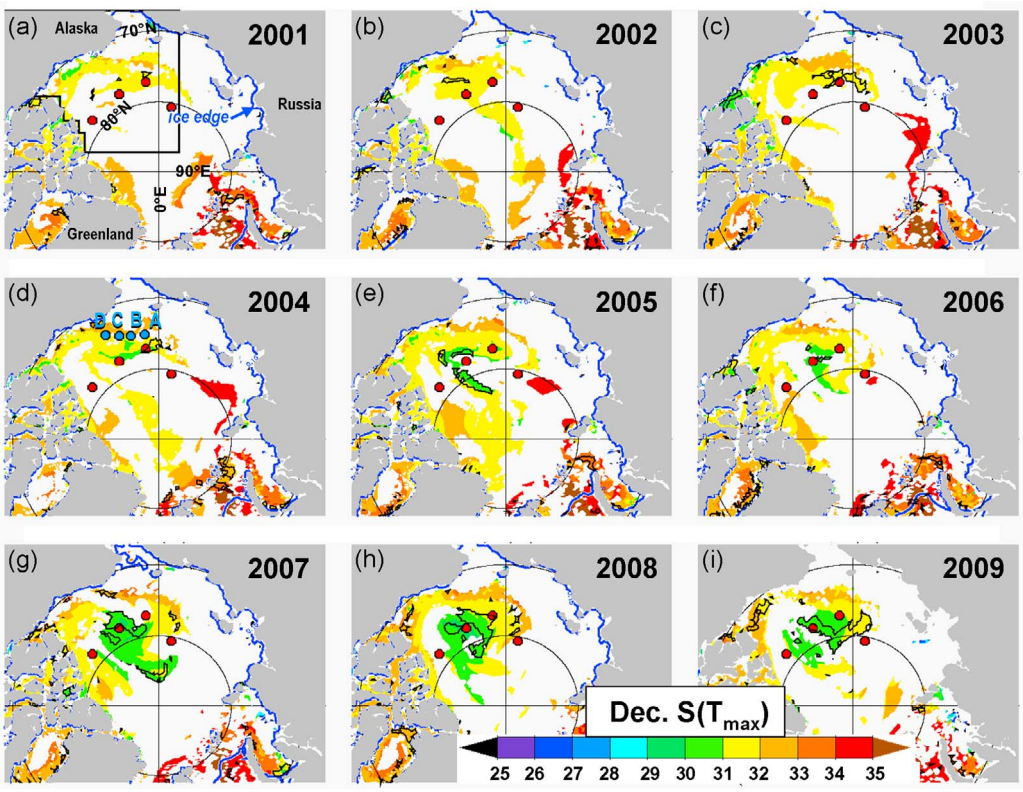

Figure 10. As in Figure 9 but for the salinity of the modeled December mean T_{max}. Here we use criteria 1 and 2 only, so that the main difference in extent between Figures 9 and 10 is the salinity threshold (i.e., criterion 3). The extent of a deeper T_{max} (satisfying criterion 1 only), which lies below the primary T_{max} within the upper 200 m, is shown as a black contour. Also shown in Figure 10a is the area over which the salinity of T_{max} is analyzed in Figure 13 (black polygon), and in Figure 10d the four locations (locations A–D) in the summer Pacific water used in Figure 12 (blue dots) are shown.

trend toward a warmer summer NSTM. A warmer summer NSTM makes it more likely to survive through the winter, but there are other factors involved. Figure 11 indicates that downwelling occurs at this location during every fall and winter, although with unusual strength in fall 2007. Thus in fall 2007 two factors combined to produce a particularly strong winter NSTM: a warm summer layer and strong fall downwelling. A third factor also plays a role; that is, increasing summer stratification (expressed in Figure 11 as a generally shallower MLD in recent years, a result largely of decreasing salinity) which tends to suppress convective mixing.

[30] Although 2007–2008 and 2008–2009 are the only winters where the "all criteria" NSTM survives intact into the next summer, other years show NSTMs that persist for a long time or even through the winter, if some of the three NSTM criteria are relaxed. Partly this is because the NSTM in some winters has only a weak temperature minimum below the T_{max} (i.e., it fails criterion 2). There is also a freshening trend in the Beaufort Gyre, evident in Figure 11 as a deepening of the S = 31 contour and noted in the observations by *Proshutinsky et al.* [2009]. This means that local summer heating in recent years is warming fresher layers that satisfy the salinity criterion 3, whereas in earlier years these warm layers would fail criterion 3. An example is the winter of 2004/2005, when an NSTM with a salinity of just over 31 persists into the summer of 2005, forming a secondary T_{max} (marked as a yellow line in Figure 11) which eventually merges at depth with the summer 2005 NSTM just after the start of 2006. This secondary T_{max} is marked in Figure 10 by a black contour.

[31] The model's 2004/2005 winter T_{max} is slightly too salty (and by late winter, has only a very small temperature minimum below it) to satisfy the "all criteria" NSTM. A similar condition is observed in other years, evident for example as the yellow area (T_{max}s with salinities between 31 and 32) in the southern Beaufort Gyre in Figure 10 and also seen as dashed red lines in Figure 11. So is this salty winter T_{max} water a locally formed NSTM, or is it a signal of summer Pacific water advected from elsewhere? Figure 11 clearly shows how this water is forming locally from summer surface heating. Given the model's salinity bias of ~1 (Figure 5), it seems likely that our results indicate that this is not summer Pacific water; rather, it is locally formed NSTM that has survived into December in the Beaufort Gyre since at least 2002 (Figure 11), although with increasing temperature in recent years.

6. NSTM and Summer Pacific Water

[32] In some years, the modeled NSTM does deepen and survive through winter and even into the following summer, forming a secondary T_{max} below a new shallower NSTM (Figures 10 and 11). However, comparison of Figures 6 and

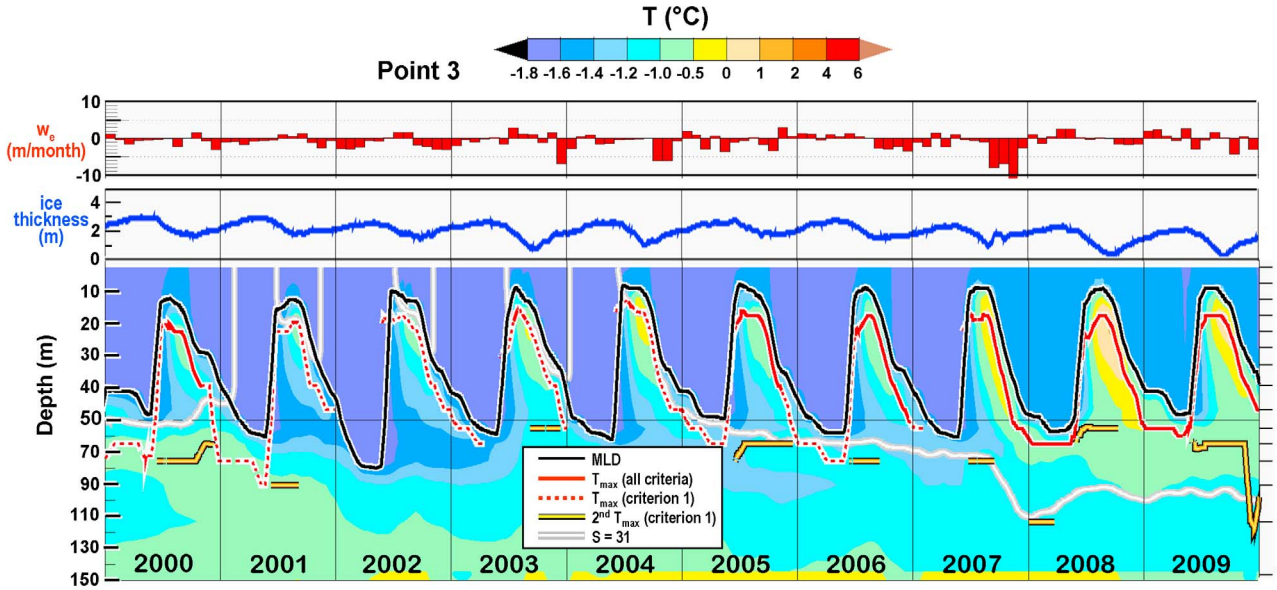

Figure 11. Similar to Figure 6b but for the years 2000–2009. In this plot the T_{max} using just criterion 1 is also plotted (red dashed line), as is a secondary deep T_{max} (yellow line) when it exists below the primary shallow T_{max}. Also, the monthly mean upwelling velocity w_e at this location is shown as a time series at the top with negative values indicating downwelling.

11 with similar plots in the work of *Jackson et al.* [2010] show that the modeled central Canadian Basin lacks a clear signal of summer Pacific water (sPW); that is, a persistent T_{max} for salinities greater than 31 at depths generally below 60 m that does not form from local surface warming. To investigate this issue further, plots similar to Figure 11 were created for all areas of the domain. Figure 12 shows an example from four points to the northwest of Alaska (marked in Figure 10d). This is the area downstream from the sPW "retroflection" where warm surface waters of Pacific Ocean origin traveling northeastward along the coast of Alaska turn abruptly northwestward and enter the anticyclonic Beaufort Gyre [*Steele et al.*, 2010], shedding eddies in the process [e.g., *D'Asaro*, 1988; *Watanabe and Hasumi*, 2009]. At some point along this pathway, the sPW encounters fresher (and thus lighter) surface waters and the subsurface T_{max} is formed.

[33] Figure 10 shows that the model does capture the formation of a sPW T_{max} along this pathway with salinity greater than 31. The model location "point A" has the greatest frequency of subsurface secondary T_{max}s (marked by yellow lines in Figure 12a and a black contour in Figure 10) in the modeled Canadian Basin. A careful examination of nearby points indicates that these originate from summertime surface warming upstream from point A. An example is the fall 2004 anomaly marked by an arrow in Figure 12a with a salinity of 32.5–33 (not shown) which can be traced upstream through points B, C, and D to surface heat input in the summer of 2003 near the northwestern Alaskan shelf break.

[34] So what is going on here? Although it lacks the horizontal resolution to resolve eddies, the model is simulating a reasonably realistic pathway and salinity of summer Pacific water [*Jones et al.*, 1998; *Steele et al.*, 2004]. This warm water enters the Beaufort Gyre north-northwest of Alaska, where it descends beneath fresher surface water to form a T_{max}. However, this temperature maximum is not as persistent (in time) or as widespread (in space) as that found in the observations [*Coachman and Barnes*, 1961; *Jackson et al.*, 2010; *Steele et al.*, 2004]. Why is this? The answer is model vertical resolution (shown on the right-hand side of Figure 12) which is too coarse to resolve the ~25 m thick sPW layer [*Jackson et al.*, 2010; *Steele et al.*, 2004] at depth levels below 60 m. The model captures the early stages of sPW T_{max} formation, descent, and lateral advection in the open water to the south of the ice edge along points A–D (see also Figure 8b), but this layer does not persist once it reaches its neutral buoyancy level owing to inadequate vertical resolution (and possibly also horizontal resolution) which is generally associated with overly strong mixing.

[35] In summary, both observations [e.g., *Jackson et al.*, 2010] and our model output indicate that it is possible to find two T_{max} layers in the upper 100 m of the Canadian Basin. One is formed locally during summer in the relatively fresh surface waters of the deep basin during recent sea ice retreat and/or thinning. This NSTM layer can survive through winter by Ekman downwelling in the center of the Beaufort Gyre. A second deeper temperature maximum can form either by survival of the previous year's NSTM, or by advection of saltier warm water from the Chukchi Sea which descends below the fresher surface waters of the central basin. The latter source creates an sPW layer which is difficult to accurately resolve in the PIOMAS model. This deficiency could affect the model's ability to accurately simulate some years' winter NSTM evolution, given that NSTM and sPW layers are at times observed to merge [*Jackson et al.*, 2010].

[36] Figure 10 indicates that the salinity range of winter upper Arctic Ocean T_{max}s has been increasing over the past decade, owing mostly to the recent appearance of the

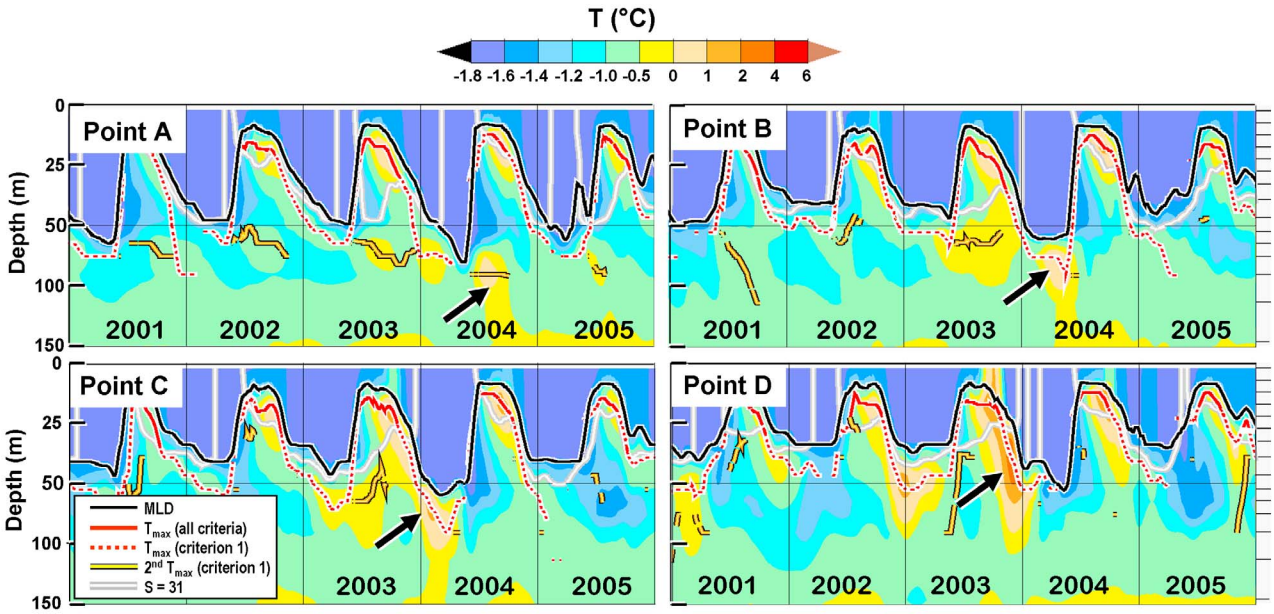

Figure 12. Similar to Figure 11 but for the years 2001–2005 at the four points A–D marked in Figure 10d. The arrows mark the secondary temperature maximum in fall 2004 at point A that can be traced back in time and space to surface heat input in the summer of 2003 near northwestern Alaska (point D).

Beaufort Gyre fresh (S < 31) NSTM. This is confirmed in Figure 13, which shows the salinity of the uppermost temperature maximum over the years 2001–2009 within a region indicated in Figure 10a. Both the model and the ITP data show an expanding salinity range which arises from an increase in fresher T_{max}s. A question might then be, can the two types of T_{max} layers (i.e., NSTM and sPW) be distinguished by their temperature and salinity alone? There is some indication from Figure 13 that the answer may be yes, given that in some recent years there is a bimodal T_{max} salinity distribution, with a minimum near the traditional threshold of S = 31. However, other tracers (e.g., nutrients) would obviously be useful to more clearly distinguish these layers.

7. Discussion

[37] What is the fate of heat absorbed from the atmosphere into the summer mixed layer of the Canadian Basin of the

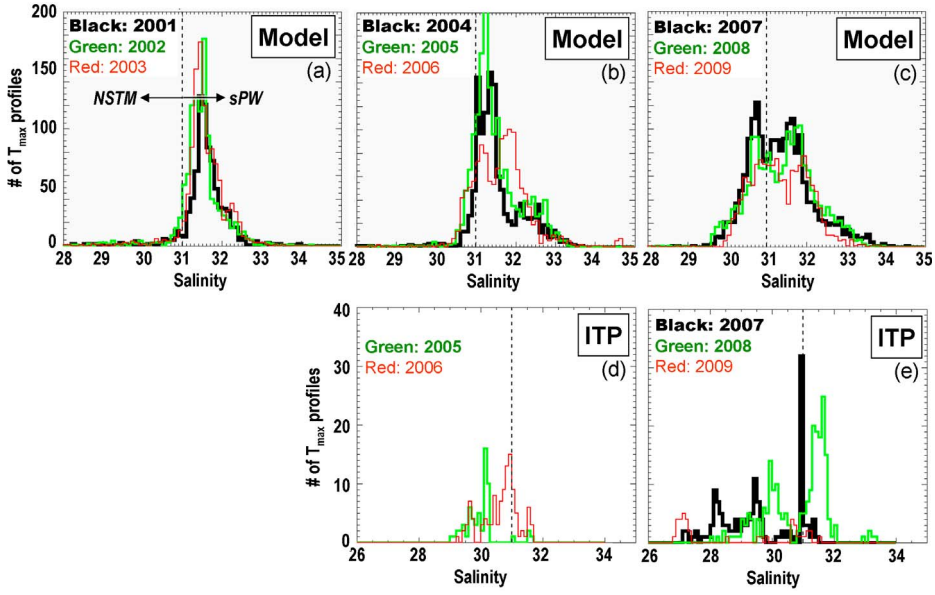

Figure 13. Salinity distribution of the uppermost ocean temperature maximum in the Canadian Basin (region shown in Figure 10a) over 2001–2009 from (a–c) the model and (d and e) ITP data. The traditional salinity minimum for sPW is shown as a vertical dashed line at S = 31; fresher T_{max}s are NSTM by the "all criteria" definition (section 3). Salinity bin size is 0.1.

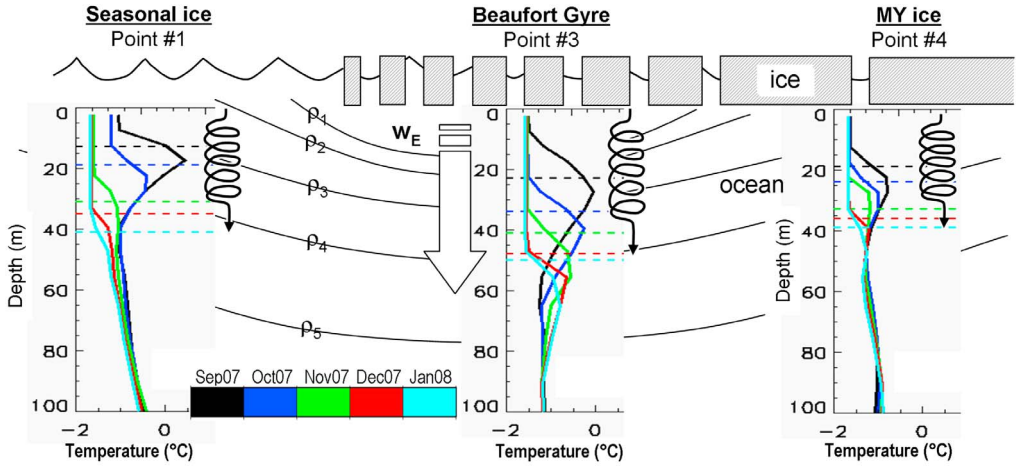

Figure 14. Temperature profiles (taken directly from Figure 2) at three locations: the seasonal ice zone (point 1 in Figure 1), the partially ice-covered, strongly stratified Beaufort Gyre (point 3 in Figure 1), and the multiyear (MY) ice pack at the edge of downwelling in the Beaufort Gyre (point 4 in Figure 1). The coiled arrows indicate the maximum depth of surface mixing (also shown as the maximum daily mixed layer depth in each month by dashed horizontal lines). Ekman downwelling in the Beaufort Gyre is indicated as w_e, and stratification in the Beaufort Gyre is indicated by additional isopycnals ρ_i.

Arctic Ocean? The answer depends on location. Figure 14 illustrates the evolution of this heat input over the fall for three locations: the seasonal sea ice pack (point 1 in Figure 1), the partially ice-covered Beaufort Gyre (point 3), and the interior ice pack at the edge of the downwelling of the Beaufort Gyre (point 4). At points 1 and 4, summer heat is completely lost to the cooling atmosphere and growing sea ice pack during the fall. At these locations, negative buoyancy flux and stress erodes the surface warm layer from the top via mixing, causing a deepening and cooling of the temperature maximum. However, fall temperature profiles stay confined within the envelope of the September profile; that is, there is no deepening of the bottom of the warm layer after summer heat input ends. At these locations, the ocean warms in the summer and cools in the fall in a largely one-dimensional (in the vertical) fashion, via air-sea exchange.

[38] One-dimensional surface erosion of the warm summer layer also happens in the Beaufort Gyre (point 3), but in addition there is downwelling forced by Ekman convergence from anticyclonic surface stress. If this downwelling is strong enough (relative to the surface mixing), it can force the NSTM below the mixed layer, so that the NSTM can persist through the winter. What is "strong enough"? Figures 2b and 6a show conditions in the seasonal ice zone where a very warm summer mixed layer was completely eroded by fall mixing forced by a cooling atmosphere and ice growth. Such a high mixing rate is not generally seen in the center of the Beaufort Gyre. This is because the region has retained at least a partial summer ice cover up to the present, which suppresses both surface stress input from the wind, as well as limits fall convection from relatively weak ice growth. Thus downwelling in the Beaufort Gyre only has to be strong enough to overcome the relatively weak surface mixing under the perennial ice pack.

[39] Why is the Beaufort Gyre NSTM becoming warmer and lasting longer into the fall and winter in recent years? First, sea ice has thinned (Figure 11) which allows more summer heating to make a warmer NSTM just below the near-surface freezing layer. Second, downwelling has increased [*Yang*, 2009], which forces the NSTM below the mixing depth during fall. The fall of 2007 was an extreme example wherein both effects were particularly strong. The following year 2008 had even less sea ice cover in the southern Beaufort Gyre, but downwelling was not as strong. The result was a slower fall deepening of the NSTM, which allowed surface mixing to rob the layer of most (but not all) of its heat by midwinter (Figure 11). Finally, a third reason for enhanced survival of the Beaufort Gyre NSTM is increased freshening in recent years [*Proshutinsky et al.*, 2009], which has increased the summer stratification and thus suppressed surface mixing.

[40] The mean sea ice circulation tends to sweep thick ice from along the Canadian Archipelago into the Beaufort Sea, so that even as the overall Arctic ice cover thins, this area may retain enough ice into the near future [*Proshutinsky et al.*, 2009; *Yang*, 2009; *Zhang et al.*, 2010a] to limit fall convection and mixing. Assuming that Ekman convergence and downwelling persist in this region, this implies that the NSTM may continue to form in the Beaufort Gyre in the near term. Further, sustained freshening of the Canadian Basin [*McPhee et al.*, 2009; *Proshutinsky et al.*, 2009] might keep NSTM salinities clearly distinguishable from the saltier sPW T_{max} layer below (Figure 13). However, the sPW itself may freshen as inputs via Bering Strait change [*Woodgate et al.*, 2006].

[41] The NSTM represents a way that the central Arctic Ocean can sequester heat absorbed locally during the summer below the winter mixed layer. Some portion of this heat has recently been surviving into the following summer within the Beaufort Gyre. Thus our model results and recent observations [*Jackson et al.*, 2010] indicate that there may be lasting effects of summertime ocean heating on the upper ocean and sea ice, in contrast to recent coupled model simulations [*Tietsche et al.*, 2011].

[42] **Acknowledgments.** We thank R. Lindsay for discussions about sea ice and J. Jackson and an anonymous reviewer for helpful comments on the first draft of this manuscript. This work is funded by the Cryosphere Program at NASA and by the Office of Polar Programs, NSF.

References

Bryan, K. (1969), Climate and ocean circulation. Part III. Ocean model, *Mon. Weather Rev.*, *97*, 806, doi:10.1175/1520-0493(1969)097<0806:CATOC>2.3.CO;2.

Coachman, L. K., and C. A. Barnes (1961), The contribution of Bering Sea water to the Arctic Ocean, *Arctic*, *14*, 147.

D'Asaro, E. A. (1988), Observations of small eddies in the Beaufort Sea, *J. Geophys. Res.*, *93*, 6669, doi:10.1029/JC093iC06p06669.

de Boyer Montégut, C., G. Madec, A. S. Fischer, A. Lazar, and D. Iudicone (2004), Mixed layer depth over the global ocean: An examination of profile data and a profile-based climatology, *J. Geophys. Res.*, *109*, C12003, doi:10.1029/2004JC002378.

Hibler, W. D. (1980), Modeling a variable thickness sea ice cover, *Mon. Weather Rev.*, *108*, 1943, doi:10.1175/1520-0493(1980)108<1943:MAVTSI>2.0.CO;2.

Hibler, W. D., and K. Bryan (1987), A diagnostic ice ocean model, *J. Phys. Oceanogr.*, *17*, 987, doi:10.1175/1520-0485(1987)017<0987:ADIM>2.0.CO;2.

Jackson, J. M., E. C. Carmack, F. A. McLaughlin, S. E. Allen, and R. G. Ingram (2010), Identification, characterization, and change of the near-surface temperature maximum in the Canada Basin, 1993–2008, *J. Geophys. Res.*, *115*, C05021, doi:10.1029/2009JC005265.

Jones, E. P., et al. (1998), Distribution of Atlantic and Pacific waters in the upper Arctic Ocean: Implications for circulation, *Geophys. Res. Lett.*, *25*, 765, doi:10.1029/98GL00464.

Krishfield, R., et al. (2008), Automated ice-tethered profilers for seawater observations under pack ice in all seasons, *J. Atmos. Oceanic Technol.*, *25*, 2091, doi:10.1175/2008JTECHO587.1.

Levitus, S. (1982), *Climatological Atlas of the World Ocean*, *Prof. Pap. 13*, 173 pp., NOAA, Silver Spring, Md.

Lindsay, R. W., and J. Zhang (2005), Thinning Arctic Sea ice: Have we passed a tipping point?, *Bull. Am. Meteorol. Soc.*, *86*, 325.

Lindsay, R. W., et al. (2009), Arctic sea ice retreat in 2007 follows thinning trend, *J. Clim.*, *22*, 165–176, doi:10.1175/2008JCLI2521.1.

Makshtas, A., D. Atkinson, M. Kulakov, S. Shutilin, R. Krishfield, and A. Proshutinsky (2007), Atmospheric forcing validation for modeling the central Arctic, *Geophys. Res. Lett.*, *34*, L20706, doi:10.1029/2007GL031378.

Maykut, G. (1982), Large-scale heat exchange and ice production in the central Arctic, *J. Geophys. Res.*, *87*, 7971, doi:10.1029/JC087iC10p07971.

Maykut, G., and M. McPhee (1995), Solar heating of the Arctic mixed layer, *J. Geophys. Res.*, *100*, 24,691.

Maykut, G., and N. Untersteiner (1971), Some results from a time-dependent thermodynamic model of sea ice, *J. Geophys. Res.*, *76*, 1550, doi:10.1029/JC076i006p01550.

McPhee, M. G., A. Proshutinsky, J. H. Morison, M. Steele, and M. B. Alkire (2009), Rapid change in freshwater content of the Arctic Ocean, *Geophys. Res. Lett.*, *36*, L10602, doi:10.1029/2009GL037525.

Min, S.-K., X. Zhang, F. W. Zwiers, and T. Agnew (2008), Human influence on Arctic sea ice detectable from early 1990s onwards, *Geophys. Res. Lett.*, *35*, L21701, doi:10.1029/2008GL035725.

Nghiem, S. V., I. G. Rigor, D. K. Perovich, P. Clemente-Colón, J. W. Weatherly, and G. Neumann (2007), Rapid reduction of Arctic perennial sea ice, *Geophys. Res. Lett.*, *34*, L19504, doi:10.1029/2007GL031138.

Parkinson, C. L., and W. M. Washington (1979), A large-scale numerical model of sea ice, *J. Geophys. Res.*, *84*, 311, doi:10.1029/JC084iC01p00311.

Perovich, D. K., B. Light, H. Eicken, K. F. Jones, K. Runciman, and S. V. Nghiem (2007), Increasing solar heating of the Arctic Ocean and adjacent seas, 1979–2005: Attribution and role in the ice-albedo feedback, *Geophys. Res. Lett.*, *34*, L19505, doi:10.1029/2007GL031480.

Perovich, D. K., J. A. Richter-Menge, K. F. Jones, and B. Light (2008), Sunlight, water, and ice: Extreme Arctic sea ice melt during the summer of 2007, *Geophys. Res. Lett.*, *35*, L11501, doi:10.1029/2008GL034007.

Proshutinsky, A., R. Krishfield, M.-L. Timmermans, J. Toole, E. Carmack, F. McLaughlin, W. J. Williams, S. Zimmermann, M. Itoh, and K. Shimada (2009), Beaufort Gyre freshwater reservoir: State and variability from observations, *J. Geophys. Res.*, *114*, C00A10, doi:10.1029/2008JC005104. [Printed *115*(C1), 2010].

Semtner, A. J. (1976), Numerical simulation of Arctic Ocean circulation, *J. Phys. Oceanogr.*, *6*, 409, doi:10.1175/1520-0485(1976)006<0409:NSOTAO>2.0.CO;2.

Serreze, M. C., et al. (2007), Perspectives on the Arctic's shrinking sea-ice cover, *Science*, *315*, 1533, doi:10.1126/science.1139426.

Shimada, K., et al. (2001), Varieties of shallow temperature maximum waters in the western Canadian Basin of the Arctic Ocean, *Geophys. Res. Lett.*, *28*, 3441, doi:10.1029/2001GL013168.

Smith, R. D., et al. (1992), Parallel ocean general-circulation modeling, *Phys. D*, *60*, 38, doi:10.1016/0167-2789(92)90225-C.

Steele, M., J. Morison, W. Ermold, I. Rigor, M. Ortmeyer, and K. Shimada (2004), Circulation of summer Pacific halocline water in the Arctic Ocean, *J. Geophys. Res.*, *109*, C02027, doi:10.1029/2003JC002009.

Steele, M., W. Ermold, and J. Zhang (2008), Arctic Ocean surface warming trends over the past 100 years, *Geophys. Res. Lett.*, *35*, L02614, doi:10.1029/2007GL031651.

Steele, M., J. Zhang, and W. Ermold (2010), Mechanisms of summertime upper Arctic Ocean warming and the effect on sea ice melt, *J. Geophys. Res.*, *115*, C11004, doi:10.1029/2009JC005849.

Stroeve, J., M. M. Holland, W. Meier, T. Scambos, and M. Serreze (2007), Arctic sea ice decline: Faster than forecast, *Geophys. Res. Lett.*, *34*, L09501, doi:10.1029/2007GL029703.

Tietsche, S., D. Notz, J. H. Jungclaus, and J. Marotzke (2011), Recovery mechanisms of Arctic summer sea ice, *Geophys. Res. Lett.*, *38*, L02707, doi:10.1029/2010GL045698.

Toole, J. M., et al. (2010), Influences of the ocean surface mixed layer and thermohaline stratification on Arctic Sea ice in the central Canada Basin, *J. Geophys. Res.*, *115*, C10018, doi:10.1029/2009JC005660.

Watanabe, E., and H. Hasumi (2009), Pacific water transport in the western Arctic Ocean simulated by an eddy-resolving coupled sea ice-ocean model, *J. Phys. Oceanogr.*, *39*, 2194, doi:10.1175/2009JPO4010.1.

Woodgate, R. A., K. Aagaard, and T. J. Weingartner (2006), Interannual changes in the Bering Strait fluxes of volume, heat and freshwater between 1991 and 2004, *Geophys. Res. Lett.*, *33*, L15609, doi:10.1029/2006GL026931.

Yang, J. (2009), Seasonal and interannual variability of downwelling in the Beaufort Sea, *J. Geophys. Res.*, *114*, C00A14, doi:10.1029/2008JC005084. [Printed *115*(C1), 2010].

Zhang, J. (2005), Warming of the Arctic ice-ocean system is faster than the global average since the 1960s, *Geophys. Res. Lett.*, *32*, L19602, doi:10.1029/2005GL024216.

Zhang, J., and D. Rothrock (2001), A thickness and enthalpy distribution sea-ice model, *J. Phys. Oceanogr.*, *31*, 2986, doi:10.1175/1520-0485(2001)031<2986:ATAEDS>2.0.CO;2.

Zhang, J., and D. Rothrock (2003), Modeling global sea ice with a thickness and enthalpy distribution model in generalized curvilinear coordinates, *Mon. Weather Rev.*, *131*, 845, doi:10.1175/1520-0493(2003)131<0845:MGSIWA>2.0.CO;2.

Zhang, J., and M. Steele (2007), Effect of vertical mixing on the Atlantic water layer circulation in the Arctic Ocean, *J. Geophys. Res.*, *112*, C04S04, doi:10.1029/2006JC003732.

Zhang, J., et al. (2000), Recent changes in Arctic sea ice: The interplay between ice dynamics and thermodynamics, *J. Clim.*, *13*, 3099, doi:10.1175/1520-0442(2000)013<3099:RCIASI>2.0.CO;2.

Zhang, J., et al. (2008), The role of Pacific water in the dramatic retreat of Arctic sea ice during summer 2007, *Chin. J. Polar Sci.*, *19*, 93.

Zhang, J., M. Steele, and A. Schweiger (2010a), Arctic sea ice response to atmospheric forcings with varying levels of anthropogenic warming and climate variability, *Geophys. Res. Lett.*, *37*, L20505, doi:10.1029/2010GL044988.

Zhang, J., Y. H. Spitz, M. Steele, C. Ashjian, R. Campbell, L. Berline, and P. Matrai (2010b), Modeling the impact of declining sea ice on the Arctic marine planktonic ecosystem, *J. Geophys. Res.*, *115*, C10015, doi:10.1029/2009JC005387.

W. Ermold, M. Steele, and J. Zhang, Applied Physics Laboratory, Polar Science Center, University of Washington, 1013 NE 40th St., Seattle, WA 98105, USA. (mas@apl.washington.edu)